Proceedings of the
46th IEEE Conference on Decision and Control
New Orleans, LA, USA, Dec. 12-14, 2007

FrA12.6

Position estimation of fluorescent probes in a confocal microscope

Sean B. Andersson

Abstract— Measurements of fluorescence intensity from an isolated fluorescing probe in a confocal microscope can be viewed as range-only measurements of the position of that probe. We present an analytical algorithm for determining its position from a collection of measurements taken at different locations in the plane. This algorithm, fluoroBancroft, is inspired by the Bancroft algorithm in GPS. We investigate the performance of the algorithm through simulation and compare it to the standard technique of fitting the data to a Gaussian profile. Our results indicate that the fluoroBancroft algorithm is more accurate than the fitting procedure when only a few measurements are used. Moreover the technique is typically two orders of magnitude faster in terms of computation time. These preliminary results indicate the fluoroBancroft algorithm holds promise for use in a real-time closed-loop controller to track the motion of single fluorescent probes.

I. Introduction

Single particle tracking in fluorescence microscopy has become an extremely important tool for understanding molecular processes [1], [2]. Particle tracking is typically achieved by analyzing a sequence of wide-field images obtained using a charge-coupled device (CCD) camera. The resolution of an optical microscope is limited by the Rayleigh criterion to

$$\frac{1.22\lambda}{2\text{N.A.}}$$

where λ is the wavelength of the light and N.A. is the numerical aperture of the objective lens [3]. However, the location of an isolated point-source can be determined with much higher accuracy by determining the center of the diffraction-limited image of the point source [1]. If limited to the focal plane, this technique can yield a temporal resolution on the order of milliseconds [4]. When extended to three dimensions, the temporal resolution is reduced to the range of seconds [5]. A confocal setup (and related techniques such as two-photon microscopy) operates in 3D and. because the fluorescence intensity is measured using an avalanche photodiode or photomultiplier tube, the temporal resolution on fluctuations in the fluorescence intensity is orders of magnitude faster than can be achieved in wide-field imaging. The trade-off is that the detection volume is extremely small, typically on the order of femtoliters. In recent years, researchers have begun to develop algorithms for tracking single fluorescent probes in confocal and two-photon microscopes [6]–[8]. Because measurements are taken sequentially, it is important for high-speed tracking that the position of the probe can be determined rapidly and with only a few measurements.

S. B. Andersson is with the Dept. of Aero. and Mech. Eng., Boston University, Boston, MA 02215. `sanderss@bu.edu`

The author recently introduced the fluoroBancroft algorithm for estimating the location of a fluorescent probe from intensity measurements. Its localization performance in the wide-field setting is comparable to the current standard technique of fitting a Gaussian profile to the data [9]. In this paper we apply the algorithm to the confocal setting. The algorithm relies on the fact that the fluorescence intensity depends only on the distance to the probe. Therefore, a measurement of the intensity can be interpreted as a measurement of the range to the source. The problem of position determination utilizing a collection of range measurements occurs in many engineering applications. The fluoroBancroft algorithm is inspired by Bancroft's algorithm for solving the localization problem in the global positioning system (GPS) [10].

Sub-diffraction limit localization is typically done by fitting the data to a Gaussian profile using a non-linear least-squares fit. This can provide precision on the order of 1-20 nm in a typical system [11], [12]. The algorithm was developed for the wide-field setting where images are comprised of hundreds of pixels and has been used primarily in localizing a particle in the focal plane. In this paper we also restrict ourselves to localization in the plane and compare the performance of the fitting approach with the fluoroBancroft algorithm in the confocal setting. These results indicate that the range-based approach is more effective when using a small number (4-10) of measurements. Moreover, the new algorithm is analytical, not numerical. As a result, it typically executes two orders of magnitude faster than the fitting approach.

In the next section we derive the position estimation algorithm. The derivation of fluoroBancroft follows the same basic approach as that of Bancroft's algorithm in GPS. However, unlike in the GPS problem in which two possible solutions are found, in our setting a unique solution is determined. A closed-form equation for this solution is derived. In Section III we describe the simulation technique used to compare the two estimation techniques. The results of the simulations are presented in Section IV.

II. The fluoroBancroft algorithm

In confocal fluorescence microscopy the output fluorescence intensity from a point source is the product of the illumination and detection intensity point spread functions

$$I(u,v) = \left(h_{\text{det}}(u,v)h_{\text{det}}^*(u,v)\right)\left(h_{\text{ill}}(u,v)h_{\text{ill}}^*(u,v)\right)$$

where the amplitude point spread function is

$$h(u,v) = -i\frac{2\pi nA\sin^2\alpha}{\lambda}e^{\frac{iu}{\sin^2\alpha}}\int_0^1 J_0(v\rho)e^{-\frac{iu\rho^2}{2}}\rho\,d\rho.$$

Here (u, v) are the normalized optical coordinates in the axial and lateral directions, n is the refractive index of the medium in which the fluorophore is embedded, $n \sin \alpha$ is the numerical aperture of the objective lens, A is the area of the illumination or detection aperture, λ is the illumination or emission wavelength, and J_0 is the zeroth-order Bessel function of the first kind [13]. The intensity pattern is circularly symmetric and gives rise to the familiar Airy disk in the plane. The intensity as a function of a normalized radial coordinate (scaling for the wavelength and numerical aperture of the system) is shown in Fig. 1. The intensity first falls to zero at $r = 3.83$. This radius determines the size of the central disk in the image of a diffraction limited spot and is termed one Airy unit.
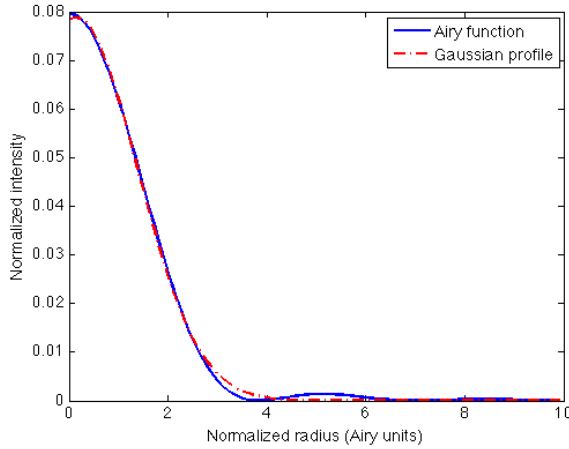

Fig. 1: Normalized output fluorescence intensity in the focal plane as a function of the normalized radial coordinate. A fitted Gaussian profile of the form (1) is superimposed on the Airy function.

Superimposed on the Airy function in Fig. 1 is a Gaussian of the form (1) fitted to the intensity profile. As can be seen, within the central disk, the intensity is well-approximated by a Gaussian. Since the Gaussian is mathematically more tractable, the intensity of a diffraction limited spot is often modeled by

$$I_{psf} = me^{-\frac{r^2}{2\sigma^2}}. \tag{1}$$

Here r is the distance between the measurement location and the fluorescent probe, m is a scaling factor determined by the total number of photons emitted by the probe during the measurement period and 2σ is the full-width, half-maximum (FWHM) of the image spot, given by

$$2\sigma = \frac{1.22\lambda}{2\sqrt{2}\text{N.A.}\ln 2}. \tag{2}$$

In this work we follow this convention and take (1) as our intensity model.

The measured intensity is given by the true intensity together with background and shot noise. The background noise, arising primarily from unwanted excited and autofluorescence of the sample, is assumed to be constant across the field of view. For the purposes of position estimation, we model it as a Gaussian random variable η_B with mean and variance equal to N_B. The shot noise is a Poisson process with a rate dependent on the total number of photons detected [1]. We assume that the photon count is high enough to model this noise as a Gaussian random variable η_{shot} with mean and variance N_{shot} equal to the sum of the intensity and the expected value of the background noise. The model for the measured intensity at a distance r away from the probe is

$$I = me^{-\frac{r^2}{2\sigma^2}} + \eta_B + \eta_{shot}. \tag{3}$$

Taking the expected value of (3) and solving for r^2 yields

$$r^2 = 2\sigma^2 \ln(2m) - 2\sigma^2 \ln(I - 2N_B). \tag{4}$$

Note that because the background noise can be measured to determine N_B, the second term on the right-hand side of (4) is known. However m is related to the true intensity of the fluorescent probe and is therefore not known. Let i index the measurements obtained from the (known) positions (x_i, y_i). The range can be expressed as

$$r_i^2 = (x_i - x_0)^2 + (y_i - y_0)^2$$

where (x_0, y_0) is the (unknown) true location of the fluorescent probe. Define

$$b \triangleq 2\sigma^2 \ln(2m), \qquad P_i^2 \triangleq 2\sigma^2 \ln(I - 2N_B)$$
$$\alpha_i \triangleq \tfrac{1}{2}\left(x_i^2 + y_i^2 + P_i^2\right), \qquad \Lambda \triangleq \tfrac{1}{2}\left(x_0^2 + y_0^2\right).$$

Then (4) can be rewritten as

$$0 = \alpha_i + \Lambda - \begin{pmatrix} x_i & y_i & 1 \end{pmatrix} \begin{pmatrix} x_0 \\ y_0 \\ b \end{pmatrix}. \tag{5}$$

Stacking together n measurements yields

$$0 = \alpha + \Lambda e - B \begin{pmatrix} x_0 \\ y_0 \\ b \end{pmatrix} \tag{6}$$

where

$$\alpha = \begin{pmatrix} \alpha_1 \\ \vdots \\ \alpha_n \end{pmatrix}, \ e = \begin{pmatrix} 1 \\ \vdots \\ 1 \end{pmatrix}, \ B = \begin{pmatrix} x_1 & y_1 & 1 \\ & \vdots & \\ x_n & y_n & 1 \end{pmatrix}.$$

Pre-multiplying (6) by B^T and rearranging yields

$$\begin{pmatrix} x_0 \\ y_0 \\ b \end{pmatrix} = B^\dagger \left(\alpha + \Lambda e\right) \tag{7}$$

where $B^\dagger = \left(B^T B\right)^{-1} B^T$ is the pseudo-inverse of B. Notice that the unknown position (x_0, y_0) appears both on the left-hand side and on the right-hand side (through Λ). Since we are interested only in the location of the fluorescent probe, we isolate the position by pre-multiplying both sides of (7) by

$$Q = \begin{pmatrix} 1 & 0 & 0 \\ 0 & 1 & 0 \end{pmatrix}.$$

This yields

$$\begin{pmatrix} x_0 \\ y_0 \end{pmatrix} = Q \left(B^\dagger \left(\alpha + \Lambda e \right) \right). \tag{8}$$

We now state an interesting property of $B^\dagger$.

Proposition 2.1: Let $e = (1, 1, \cdots, 1)^T$ and let A be a full rank $n \times 2$ matrix, $n > 2$, such that e is not in the column space of A. Define $B = \begin{pmatrix} A & e \end{pmatrix}$. Then

$$B^\dagger e = \begin{pmatrix} 0 \\ 0 \\ 1 \end{pmatrix}.$$

Proof: The result follows from a direct calculation of the pseudo-inverse. ∎

To satisfy the conditions of this proposition, at least three measurements must be used and the locations of these measurements must not be collinear. Under this assumption, applying Proposition 2.1 to (8) removes Λ from the equation and results in the solution

$$\begin{pmatrix} x_0 \\ y_0 \end{pmatrix} = QB^\dagger \alpha. \tag{9}$$

Since B and α depend only on the measurements and the locations of those measurements, (9) determines the location of the fluorescent probe as a closed-form equation.

Thus to determine the position of a fluorescent probe, one first obtains three or more measurements from different locations in space. These measurements define the matrix B and the vector α. The Moore-Penrose inverse of B is calculated and the location of the probe found from (9).

III. SIMULATION METHODS

To investigate the performance of the fluoroBancroft algorithm, we modeled a point source fluorescing at a wavelength of 540 nm at a rate of 40 photons/ms. The fluorescence was imaged using a 1.2 N.A., $20\times$ magnification objective lens through a circular pinhole onto a point detector. The signal-to-noise ratio (SNR) depends on the pinhole radius [14]. The pinhole radius was set to 2.86 μm, corresponding to approximately half an Airy unit.

The noise-free intensity value of the fluorophore in the detector plane was modeled as a Gaussian as in (3) with the parameter m determined by the fluorescence rate and the integration time (the time spent collecting photons at a single location). With the given parameters, the FWHM was 140 nm. The total number of photons collected by the detector from the fluorescent probe was determined by integrating the exponential over the area of the pinhole and multiplying the result by the quantum efficiency of the detector. Background noise was introduced by adding a sample from a Poisson process with parameter $N_B = 10$ photons/ms. Finally, shot noise was included by adding a sample from a Poisson distribution whose parameter was given by the total number of photons collected by the detector. For a small circular pinhole, the SNR for the model taken here can be shown to be given approximately by [14]:

$$\text{SNR} = \sqrt{Q_E n_p} \frac{\pi r_d \text{N.A.}}{\lambda \text{M} \sqrt{1 + N_B/N}}$$

where N is the fluorescence rate of the molecule, λ is the wavelength of the emitted fluorescence, M is the magnification of the objective, Q_E is the quantum efficiency of the detector, and n_p is the total number of photons emitted by the molecule during the integration time. For all simulations, Q_E was set to 0.55 and an integration time of 15 ms was chosen, leading to a signal-to-noise ratio of approximately 17.

In Fig. 2 we show the simulated measured fluorescence signal measured along a radial line. The fluorescent probe was located at the origin and measurements were taken at every 10 nm. Given that $N_B = 10$ photons/ms, the integration time was 15 ms, and the presence of the shot noise, the expected fluorescence level in the absence of a fluorophore is 300 photons. From the theoretical model, the fluorescence signal from the probe drops to zero at one Airy unit, corresponding to approximately 274 nm for the parameters chosen here. As seen in Fig.2, the signal falls to the noise floor at approximately 300 nm as expected.
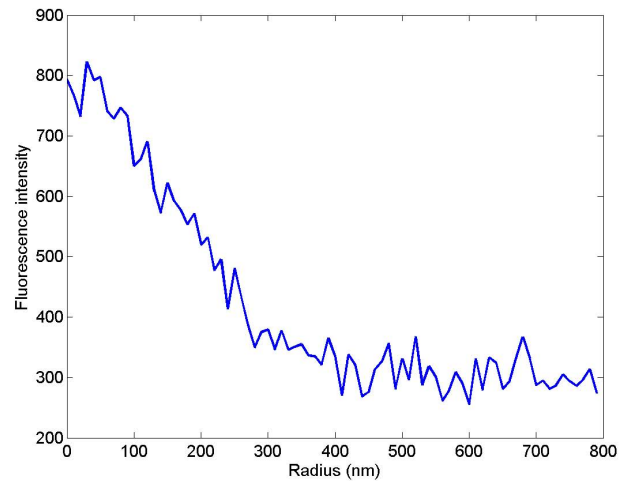

Fig. 2: Simulated intensity measurements along a radial line with an SNR of 16.2 The fluorescent probe is located at the origin.

For each simulation run, the location of the fluorescent probe was determined by sampling from a uniform density on a circle centered on the origin and with radius r_d where r_d is the radius of the pinhole projected back into the sample plane.

Intensity measurements were made from different positions in the plane and then used to estimate the location of the fluorescent probe. Measurement positions were approximately uniformly spaced around a circle centered on the origin. Because the location of the probe was unknown, the radial distance for each measurement location was selected randomly from a uniform distribution on $[0, r_d]$. This sampling pattern ensured measuring the fluorescence intensity at several different ranges to the fluorescent probe. An example for the case with eight measurements is shown in Fig. 3. The circle drawn on the figure denotes the region over which the probe might be. We note that the problem of optimal

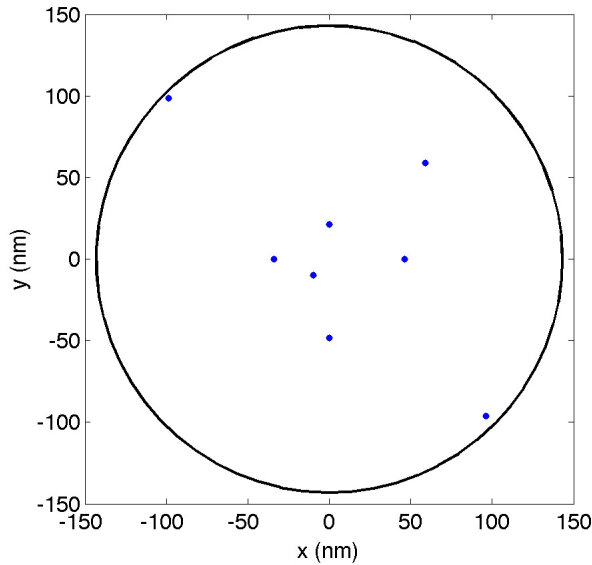selection of measurement locations remains open.

Fig. 3: Typical pattern of measurement locations. Locations are selected approximately uniformly spaced around a circle. The radial distance to each location is selected randomly from a uniform distribution from $[0, r_d]$. The fluorescent probe is located at an unknown location inside the circle.

For every fixed number of measurements, 500 iterations of the simulation were run. The location of the fluorescent probe was determined using the fluoroBancroft algorithm (9) as well as by using a nonlinear least-squares fit of the data to a Gaussian given by

$$I(x, y) = Ae^{-\frac{(x-x_0)^2+(y-y_0)^2}{2\sigma^2}}$$

in which x_0, y_0, A and σ were allowed to vary. The simulations were performed in Matlab and the Gaussian fit performed using the built-in routine `lsqnonlin`. Because there are three unknowns (the location of the fluorescent probe in the plane and the number of photons emitted by the fluorophore), at least three independent measurements are needed to produce a unique answer. Additional measurements help to reduce the error and standard deviation of the estimates. In this study, simulations were run with from four to 36 measurements (that is from every 90° to every 10°).

IV. RESULTS AND DISCUSSION

Fig. 4 shows the standard deviation of the error across the 500 iterations for both fluoroBancroft and the Gaussian fit algorithm. As the figure shows, the fluoroBancroft algorithm is accurate relative to the Rayleigh criterion across the range of numbers of measurements. The Gaussian fit approach has a larger standard deviation than fluoroBancroft for the entire range of numbers of measurements. From (2), the FWHM for the simulations parameters is approximately 200 nm. Therefore for less than eight measurements, the standard deviation of the fit is larger than the FWHM of the point
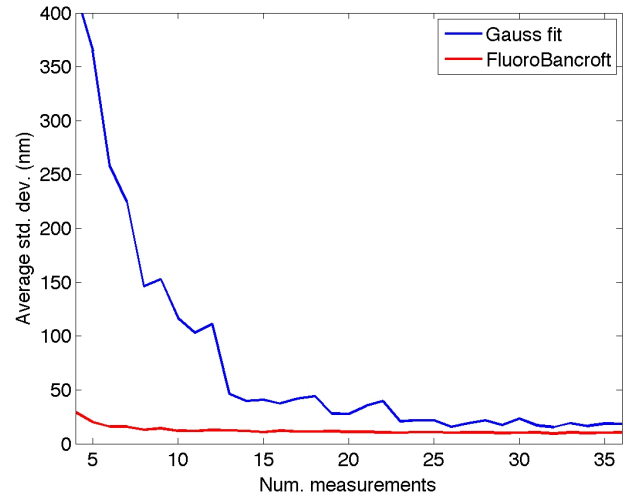

Fig. 4: Standard deviation of the position estimates of the fluorescent probe. The simulations indicate that the fluoroBancroft algorithm performs very well even with only four measurements while Gaussian fit technique needs approximately 20 measurements to achieve similar performance. Moreover, when less than eight measurements are used, the Gaussian fit error is larger than the Rayleigh resolution criterion, indicating that the algorithm is yielding no information.
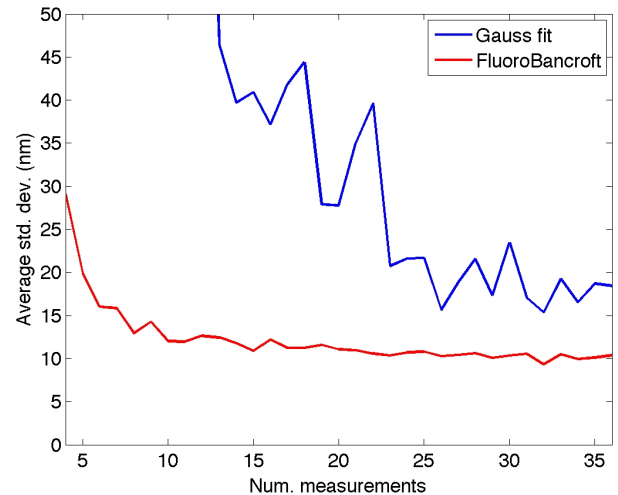

Fig. 5: Standard deviation of the position estimates of the fluorescent probe, zoomed in the vertical direction to show the performance of the fluoroBancroft algorithm. The standard deviation of the fluoroBancroft algorithm is less than 30 nm even with only four measurements and improves, albeit slowly, as more measurements are used. The Gaussian fit approach improves rapidly as more measurements are added until about 20 data points are used.

spread function. This implies that the technique fails to localize the fluorescent probe. Fig. 5 shows the same data but now magnified in the vertical direction. The results indicate that the fluoroBancroft algorithm has a standard deviation of less than 30 nm, significantly below the diffraction limit, even when using only four measurements. The standard deviation quickly improves as measurements are added up to approximately 10 measurements. After that, the rate of improvement is slow. By contrast the standard deviation of the Gaussian fit drops quickly as more measurements are added up to approximately 20 measurements. After this the two algorithms have similar rates of improvements. It should be noted that in a previous simulation study based on CCD imaging, the Gaussian fit was shown to have a lower standard deviation than the fluoroBancroft approach when large data sets (larger than 64 measurement locations) were used [9].

The mean of the absolute error in the measurement is shown in Figs. 6 and 7. The fluoroBancroft algorithm has a small error of approximately 35 nm even with only four measurements. However, the rate of decrease in this error is extremely slow. The Gaussian fitting approach has an initially high error, once again indicating that the method is unable to localize the fluorescent molecule based only on a few measurements. However, the error rapidly decreases and after approximately 17 measurements, it outperforms the fluoroBancroft approach.
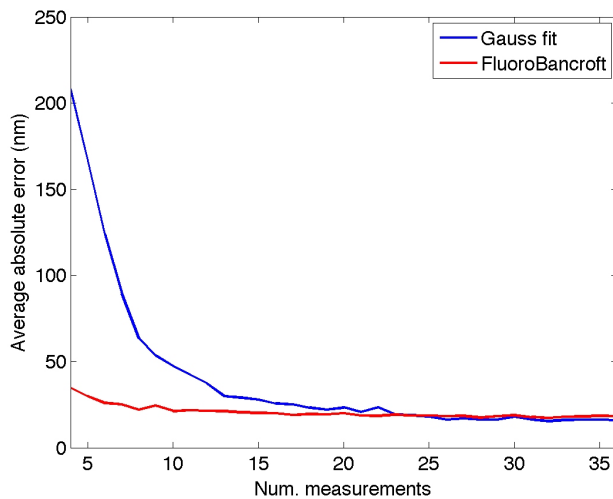

Fig. 6: Absolute error in the position estimates of the fluorescent probe. The error in the fluoroBancroft algorithm slowly decreases as more measurements are used. The Gaussian fit approach error decreases rapidly until approximately 12 measurements. After that the rate of improvement is similar to the fluoroBancroft algorithm.

Because one of the main goals of this estimator is in a closed-loop tracking system, it is important to consider the execution time of the algorithm. All calculations were done using Matlab. Because Matlab is typically slower than a custom program, the exact times are not meaningful. However, the ratio provides a rough measure of the relative
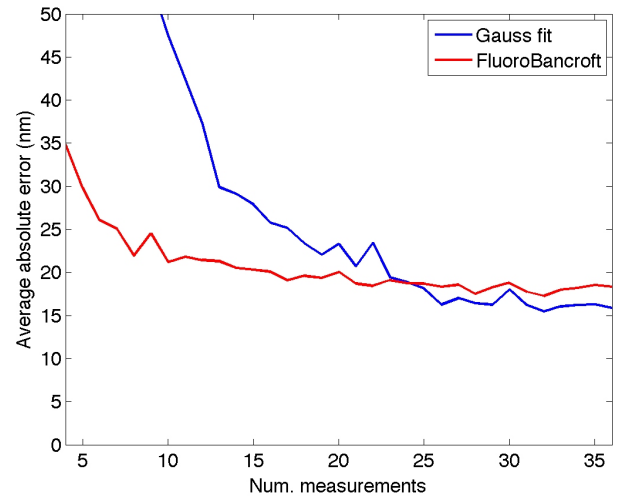

Fig. 7: Absolute error in the position estimates of the fluorescent probe, zoomed in the vertical direction to more clearly show the performance of the algorithms with larger numbers of measurements.

computational complexity. The resulting ratio is shown in Fig. 8. The figure indicates that fluoroBancroft is two to three orders-of-magnitude faster than the fitting procedure. Moreover, because the fitting process is a numerical optimization, the execution time depends upon the initial conditions, the SNR, and the number of measurements and can vary widely.
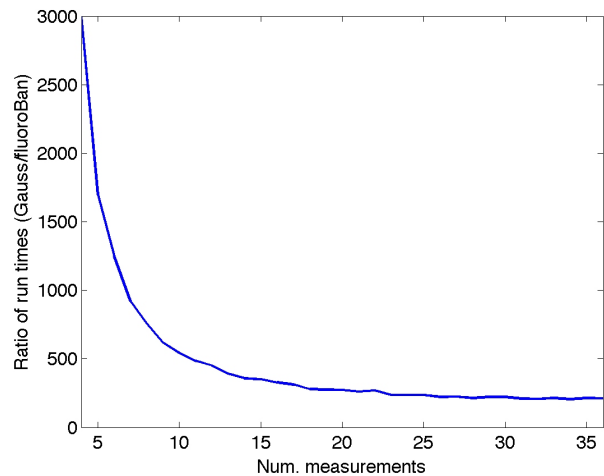

Fig. 8: Ratio of execution times of the Gaussian fit procedure to the fluoroBancroft algorithm. The execution time for fluoroBancroft is generally two orders of magnitude lower than that of the numerical approach.

One aspect which this study did not consider was the effect of the choice of measurement location on the accuracy of the estimation. However it is to be expected that this plays an important role in the performance of the algorithms,

particularly when only a few measurements are used. It is clear that measurements at a range of more than one Airy unit from the fluorescent probe will consist almost entirely of noise. However even when all measurements are within one Airy unit, the location will influence the accuracy and may possibly result in a bias as well. Fig. 9 indicates some dependence of the error on the measurement locations. In this figure the mean error in the x and y directions are shown as a function of the number of measurements. Although the mean error is small, it does appear to vary in a somewhat regular pattern, indicating the need for further theoretical and experimental study.
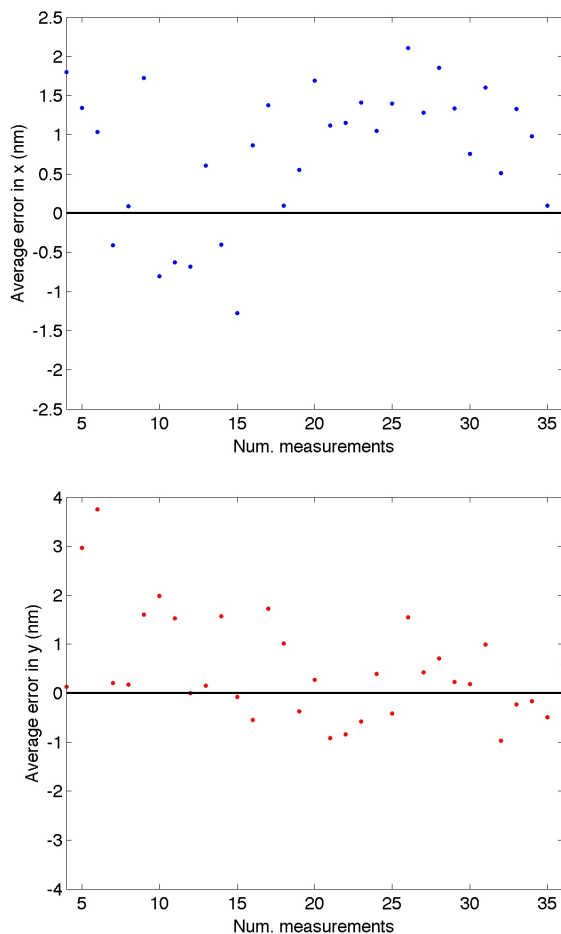

Fig. 9: Mean of the errors in the x (top) and y (bottom) directions. These results indicate that some bias may be introduced into the estimate depending on the choice of sampling pattern.

V. Conclusion

In this paper we have presented a new algorithm for sub-diffraction limit estimation of the position of a fluorescing probe. It was compared in simulation to the current standard approach of fitting a Gaussian to the data to determine the center of the diffraction spot. This study indicates that the new algorithm is both more accurate and more computationally efficient than the fitting procedure when only a few

measurements are used in the estimation. It is expected that this approach will be useful in closed-loop algorithms for tracking single fluorescing probes.

These preliminary results are promising but a theoretical analysis of the algorithm still needs to be performed to understand the bias and variance properties of the estimator and to develop sampling patterns which optimize the performance. It is also important to note that both the intensity and noise models are rough approximations. Better performance is expected once more faithful models are developed. In on-going work, the fluoroBancroft algorithm has been extended to three-dimensional localization and similar studies in that setting are being carried out.

VI. Acknowledgements

References

[1] M. K. Cheezum, W. F. Walker, and W. H. Guilford, "Quantitative comparison of algorithms for tracking single fluorescent particles," *Biophys. J.*, vol. 81, no. 4, pp. 2378–2388, October 2001.

[2] H. P. Babcock, C. Chen, and X. Zhuang, "Using single-particle tracking to study nuclear trafficking of viral genes," *Biophys. J.*, vol. 87, no. 4, pp. 2749–2758, October 2004.

[3] S. Inoué, *Handbook of biological confocal microscopy*, 3rd ed. Springer, 2006, ch. 1. Foundations of confocal scanned imaging in light microscopy, pp. 1–14.

[4] C. Kural, H. Kim, S. Syed, G. Goshima, V. I. Gelfand, and P. R. Selvin, "Kinesin and dynein move peroxisome in vivo: a tug-of-war or coordinated movement?" *Science*, vol. 308, no. 5727, pp. 1469–1472, June 2005.

[5] D. Thomann, D. R. Rines, P. K. Sorger, and G. Danuser, "Automatic fluorescent tag detection in 3D with super-resolution: application to the analysis of chromosome movement," *J. Microsc.*, vol. 208, no. 1, pp. 49–64, October 2002.

[6] V. Levi, Q. Ruan, and E. Gratton, "3-D particle tracking in a two-photon microscope: application to the study of molecular dynamics in cells," *Biophys. J.*, vol. 88, no. 4, pp. 2929–2928, April 2005.

[7] A. J. Berglund and H. Mabuchi, "Feedback controller design for tracking a single fluorescent molecule," *Appl. Phys. B*, vol. 78, no. 5, pp. 653–659, March 2004.

[8] S. B. Andersson, "Tracking a single fluorescent molecule with a confocal microscope," *Appl. Phys. B*, vol. 80, no. 7, pp. 809–816, June 2005.

[9] ——, "Precise localization of fluorescent probes without numerical fitting," in *Proceedings of the IEEE International Symposium on Biomedical Imaging (ISBI)*, 2007, pp. 252–255.

[10] S. Bancroft, "An algebraic solution of the GPS pseudorange equations," *IEEE Trans. Aerosp. Electron. Syst.*, vol. AES-21, pp. 56–59, November 1985.

[11] R. E. Thompson, D. R. Larson, and W. W. Webb, "Precise nanometer localization analysis for individual fluorescent probes," *Biophys. J.*, vol. 82, no. 5, pp. 2775–2783, May 2002.

[12] C. Kural, H. Balci, and P. R. Selvin, "Molecular motors one at a time: FIONA to the rescue," *J. Phys. Condens. Matter*, vol. 27, no. 47, pp. S3979–S3995, 2005.

[13] J. E. Jonkman and E. H. K. Stelzer, *Confocal and two-photon microscopy. Foundations, applications, and advances*. Wiley-Liss, 2002, ch. 5. Resolution and Contrast in Confocal and Two-photon microscopy, pp. 101–125.

[14] C. J. R. Sheppard, X. Gan, M. Gu, and M. Roy, *Handbook of biological confocal microscopy*, 3rd ed. Springer, 2006, ch. 22: Signal-to-noise in confocal microscopes, pp. 363–370.